Associates, whose patience and technical guidance have been a constant source of inspiration.

References

[1] J. T. McGoogan, L. S. Miller, G. S. Brown, and G. S. Hayne, "The S-193 radar altimeter experiment," *Proc. IEEE*, vol. 62, pp. 793–803, June 1974.

[2] R. K. Moore and C. S. Williams, Jr., "Radar terrain at near vertical incidence," *Proc. IRE*, vol. 45, pp. 228–238, Feb. 1957.

[3] J. K. Schindler, "Electromagnetic scattering phenomena associated with extended surfaces," *IEEE Internatl. Conv. Rec.*, vol. 15, part 2, pp. 136–149, 1967.

[4] W. J. Pierson and E. Mehr, "The effects of wind waves and swell on the ranging accuracy of a radar altimeter," Rept. on Contract No. N62306-70-A-0075, New York University, School of Engineering and Science, Jan. 1970.

[5] L. S. Miller and G. S. Hayne, "System study of the geodetic altimeter concept," final rept. on NASA Contract No. NAS6-1829, Research Triangle Institute, March 1971.

[6] ——, "Characteristics of ocean reflected short radar pulses with applications to altimetry and surface roughness determination," in *Sea Surface Topography from Space*, vol. 1, J. R. Apel, Ed., NOAA Tech. Rept. ERL 228-AOML 7, pp. 12-1 to 12-17, May 1972.

[7] T. Berger, "Satellite altimetry using ocean backscatter," *IEEE Trans. Antennas Propagat.*, vol. AP-20, pp. 295–309, May 1972.

[8] G. S. Brown, "Reduced backscattering cross section (σ°) data from the Skylab S-193 radar altimeter," NASA-CR 141401, Applied Science Associates, Apex, NC, Oct. 1975.

[9] J. E. Seltzer, "Spatial densities for specular points on a Gaussian surface," *IEEE Trans. Antennas Propagat.*, vol. AP-20, pp. 723–730, Nov. 1972.

[10] L. S. Miller and G. S. Brown, "Engineering studies related to the GEOS-C radar altimeter," NASA CR-137462, Applied Science Associates, Apex, NC, May 1974.

[11] A. H. Schooley, "Upwind-downwind ratio of radar return calculated from facet size statistics of a wind-disturbed water surface," *Proc. IRE*, vol. 50, pp. 456–461, April 1962.

[12] F. B. Hildebrand, *Introduction to Numerical Analysis.* New York: McGraw-Hill, 1956, pp. 378–382.

[13] G. S. Brown, "Interpretation of anomalous scattering data obtained from the Skylab radar altimeter," Tech. Memo, NASA Contract NAS6-2520, Applied Science Associates, Apex, NC, Oct. 1975.

[14] T. Hagfors, "Backscattering from an undulating surface with applications to radar returns from the moon," *J. Geophys. Res.*, vol. 66, pp. 777–785, 1961.

[15] G. S. Hayne, L. S. Miller, and G. S. Brown, "Altimeter waveform software design," final report on Task 3.1 of NASA Contract No. NAS6-2520, Applied Science Associates, Inc., Apex, NC, April 1975.

[16] D. E. Weissman, "Two frequency radar interferometry applied to the measurement of ocean wave height," *IEEE Trans. Antennas Propagat.*, vol. AP-21, pp. 649–656, Sept. 1973.

[17] G. A. Campbell and R. M. Foster, *Fourier Integrals for Practical Applications.* New Jersey: Van Nostrand, 1948.

Dual Frequency Correlation Radar Measurements of the Height Statistics of Ocean Waves

DAVID E. WEISSMAN, SENIOR MEMBER, IEEE, AND JAMES W. JOHNSON

***Abstract*—A radar technique has been developed for measuring the statistical height properties of a random rough surface. This method is being applied to the problem of measuring the significant wave height and probability density function of ocean waves from an aircraft or spacecraft. Earlier theoretical and laboratory results have been extended to define the requirements and performance limitations of flight systems. Some details of the current airborne radar system are discussed and results obtained on several experimental missions are presented and interpreted.**

I. Introduction

A FLIGHT program is underway to explore and develop the usefulness of the dual frequency correlation radar for measuring the significant wave height and the statistical height properties of the ocean surface. Namely, the probability density function of the specular point heights and its root mean square value are measured. This technique is described in a paper by Weissman [1]. The method rests on the assumption that a rough ocean surface will backscatter normally incident microwave energy as the sum of contributions from numerous independent specular points. The characteristic property of this technique is that it measures the spread in range of the incoherent specular points. Measurement accuracy can be affected by the inherent sphericity of the illuminating electromagnetic wave and any additional range spread induced by off nadir alignment of the antenna beam axis. These effects cause points at identical heights relative to the mean planar surface to differ in range to the point where the radar is situated. Previous theoretical analysis is extended and attention has been directed to determining the properties of an airborne system for making measurements over a range of sea surface conditions. The theoretical approach is demonstrated and calculations that bear on the measurement and design problem are presented.

The method of signal processing is reconsidered and the advantages of modifications that simplify the flight instrument are examined. These results are supported by additional laboratory measurements, extending those presented earlier [1]. The laboratory results can also be

Manuscript received September 22, 1975; revised May 10, 1976.

D. E. Weissman is with the Dept. of Engineering and Computer Sciences, Hofstra University, Hempstead, NY 11550.

J. W. Johnson is with NASA Langley Research Center, Hampton, VA 23665.

interpreted to answer questions about the relation of the statistics of the returned signal to the geometry of the illuminated surface.

Aircraft measurements to evaluate this technique under actual open ocean conditions have been made. This effort involved a modification and addition to the AAFE RADSCAT scatterometer system that is mounted on a C-130 NASA Aircraft. Details of the flight instrument and its operation are discussed. Ocean wave height observations have been made for wind conditions of 3 to 55 knots, and the ability of the flight instrument (usually referred to as the dual frequency scatterometer (DFS)) to infer true rms and significant wave height is clear. In addition, these data validate the theoretical approach that predicts the effect of antenna beamwidth and off nadir alinement. Measurement programs are continuing. These will combine aircraft (high altitude DFS and low altitude scatterometry) and surface truth observations (laser profilometers and wave riders). From these, the effect of the sea surface geometry and the variability of the scattering cross section with surface elevation on the instrument accuracy can be determined. Optimum instrument and antenna beam geometry parameters are discussed and future applications are considered.

II. Generalization of Earlier Analysis

The analytical basis for this technique is an application of the physical optics approximation to the Kirchhoff–Huygens integral. The calculation of the backscattered field for a highly directional source is presented in [1]. This includes the Fresnel approximation in the evaluation of the integrals by the stationary phase approximation, which yields a received field that is the sum of contributions from individual specular points. A desired extension here for aircraft applications is to allow the axis of the narrow beam antenna to tilt off nadir by any amount. The only restriction is that the radius of the illuminated area should be much less than the one way range between the radar and the point where the beam axis intercepts the surface. This mathematical restriction would become important only near grazing angles.

The dual frequency technique is basically analogous to the impulse radar in that it measures the spread in ranges of the incoherent, randomly distributed targets that are illuminated. But unlike the impulse radar, which measures this range spread by observing the width of the time response, the dual frequency radar senses the average phase difference among the targets at two separated frequencies. The accuracy of this method can be degraded by the sphericity of the incident wave in the illuminated area and the range spread induced by an off nadir alinement of the antenna beam. This causes points at identical heights with respect to the mean planar surface to differ in range to the point where the radar is situated. These effects produce a decorrelation factor that multiplies the roughness decorrelation and causes a reduction of the total measured correlation. The pattern effect with nadir alinement was included in the theoretical development of [1].

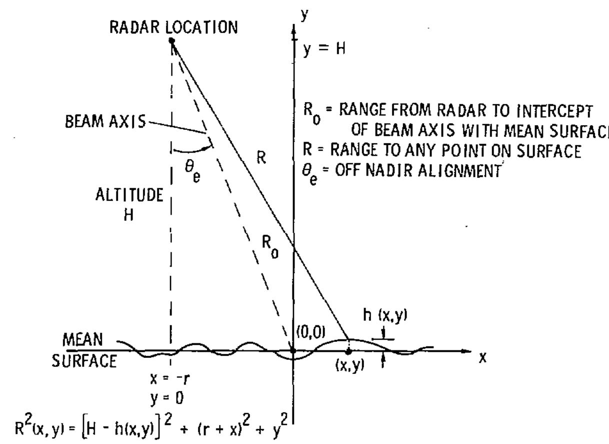

Fig. 1. Coordinate system for off-nadir analysis.

To generalize this analysis for any angle of incidence, the coordinate system shown in Fig. 1 is used. The origin is taken to be the point where the beam axis intercepts the mean surface. The steps in the analysis to compute the decorrelation term will be identical except that the range term of eq. (6) in [1] will be replaced by a new term determined from Fig. 1,

$$R = [(H - h(x,y))^2 + (r + x)^2 + y^2]^{1/2}.$$

Letting $H^2 + r^2 \triangleq R_0^2$, $r = R_0 \sin\theta_e$, and assuming R_0 is much larger than any value of $x^2 + y^2$, the distance from any point that will be illuminated to the origin becomes,

$$R \cong R_0 - h\cos\theta_e + x\sin\theta_e + \frac{x^2 + y^2}{2R_0}.$$

The new term that represents the decorrelation effect caused by the range spreading due to the illumination geometry (extension of eq. (19) of [1]) is

$$R_p(\Delta k) = \left\langle \exp\left[j2(\Delta k)\left(x\sin\theta_e + \frac{x^2 + y^2}{2R_0}\right)\right] G_1^2 G_2^2 \right\rangle. \quad (1)$$

The angular brackets represent the expectation with respect to the probability density function for the density of specular points distribution in the illuminated area. The computations will employ the assumption that the density of specular points is constant throughout this area. This situation is not expected to always be accurate since some clustering of specular points would be expected near the peaks and troughs. Nonetheless, it is a reasonable approximation and suitable for discussing the main features of the decorrelation term. For $\theta_e = 0°$, $R_p(\Delta k)$ reduces to $P(\Delta k)$ in [1]. For values of $\theta_e > 20°$, it is necessary to deal with distributions of Bragg scatterers, but the general approach will be unchanged.

Consideration of the effect of changes in the pattern shape with frequency have indicated that it is safe to assume that the antenna pattern functions G_1 and G_2 are identical, and Gaussian beam shapes will be chosen for purposes of calculation. Therefore

$$G_1^2 = G_2^2 = G_0^2 \exp\left[-0.69\left(\frac{x^2+y^2}{r_1^2}\right)\right]$$

where r_1 is the radius on the mean surface of a circle centered at the origin where the illumination power density is 3 dB below the maximum level. Denoting the angular 3 dB beamwidth as θ_b,

$$r_1 = \frac{R_0\theta_b}{2\cos\theta_e}.$$

The evaluation of this decorrelation term is performed by recognizing that the p.d.f. for the distribution of specular points is the ratio of the density of specular points to the total number in a large sample area, n_A/N. Then (1) becomes

$$\frac{n_A}{N}\int_{-Y_M}^{+Y_M}\int_{-X_M}^{+X_M} dx\, dy \cdot \left[\exp j2(\Delta k)\left(x\sin\theta_e + \frac{x^2+y^2}{2R_0}\right)\right] G_0^4 \cdot \exp\left[-1.38\left(\frac{x^2+y^2}{r_1^2}\right)\right]. \tag{2}$$

The sample area, $4X_MY_M$, can be selected as large as desired so that the limits of integration can be considered to be plus and minus infinity. The integration then becomes straightforward, and the expression derived from (2) is normalized by its value at $\Delta k = 0$ to yield the complete decorrelation term,

$$R_p(\Delta k) = \left(\frac{\beta}{\beta - j\alpha}\right)\exp\left[-\frac{\gamma^2}{4(\beta - j\alpha)}\right] \tag{3}$$

where

$$\beta = \frac{1.38}{r_1^2} \qquad \alpha = \frac{\Delta k}{R_0} \qquad \gamma = 2\Delta k\sin\theta_e.$$

In general $R_p(\Delta k)$ is a complex function with a magnitude and phase angle that vary with Δk. In the event that only the magnitude is of interest in a particular measurement, it can be expressed as

$$|R_p(\Delta k)| = \frac{1}{\sqrt{1+u^2}}\exp\left[-\frac{u^2}{1+u^2}(1.38)\frac{(\sin 2\theta_e)^2}{\theta_b^2}\right] \tag{4}$$

with

$$u = \frac{\alpha}{\beta} = \frac{(\Delta k)H\theta_b^2}{5.52\cos^3\theta_e}.$$

When the magnitude of the two-frequency correlation function is measured, it is seen to depend on the roughness term expressed as the characteristic function or Fourier transform of the p.d.f. for the height of the specular points, $p(h)$ and $|R_p|$, respectively,

$$|R(\Delta k)| = |\langle\exp[j2(\Delta k)h\cos\theta_e]\rangle||R_p(\Delta k)|$$

$$|R(\Delta k)| = \left|\int_{-\infty}^{\infty} p(h)\exp[j2(\Delta k)h\cos\theta_e]\, dh\right| |R_p(\Delta k)|. \tag{5}$$

For example, when the height distribution of specular points is Gaussian, with a root mean-square value of σ, then

$$p(h) = \frac{\exp\left(-\frac{h^2}{2\sigma^2}\right)}{\sqrt{2\pi}\,\sigma}$$

and

$$|R(\Delta k)| = \exp[-2(\Delta k\sigma\cos\theta_e)^2]|R_p(\Delta k)|. \tag{6}$$

The greater the roughness parameter σ, the narrower this function will appear on a graph when plotted versus Δk (or Δf). It should be noted that when $p(h)$ is symmetrical, the roughness term (characteristic function) has no phase function; therefore, the magnitude of $R(\Delta k)$ is sufficient to yield $p(h)$ upon inversion. This procedure was followed with the measurements that have been performed. On the other hand, if $p(h)$ is unsymmetrical, its characteristic function will introduce a phase term into $R(\Delta k)$ which in turn must be measured in order to reconstruct $p(h)$ exactly. This phase measurement for $R(\Delta k)$ would require additional complexity in the system, but could be accomplished if necessary.

Attention is now directed to the assumed properties of the reflectivity of the specular points. It should be kept in mind that the two-frequency correlation function senses the density and the relative cross section of the scattering elements (specular points) along the propagation path of the radar wave [2], [3]. In effect, the scattering cross section per unit area as a function of depth (or range) is observed. With the assumption that all the specular points have the same cross section, this scattering distribution reduces to that of the propulation of specular points at different heights at the surface, which is represented by the probability density function. Kodis [4] has shown that the strength of the field backscattered by each specular point depends on the surface curvature at that location. This can be expected to vary with elevation and to exhibit some random fluctuation at a given elevation for an actual sea surface sample. The theoretical analysis that leads to the derivation of the two-frequency correlation function in [1] permits the inclusion of this effect in the theoretical prediction when a statistical description of the behavior of this curvature has been formulated. This formulation does not yet exist in quantitive form, but some qualitative information is available from the results obtained by Yaplee *et al.* [5]. Their X-band measurements at the Chesapeake light tower were able to resolve reflectivity (incoherent) as a function of depth (impulse power response) and were able to separate the effects due to specular point populations at the crest and the trough from the differences in curvature at these locations. The variation in reflectivity versus elevation due to curvature is presented in their Figs. 9 and 10, and these observations indicate a noticeable increase towards the wave trough, but the amount of asymmetry diminishes with the wind speed and wave height. Since the majority of the scatterers exist near the surface mean, the net effect on the cross section per unit area distribution as a function of elevation is to induce a relatively minor asymmetry as seen in their Figs. 11 and 12.

The result embodied in (6) is well supported by the flight and laboratory data and also serves as an important guide in determining what beam and aircraft geometry is needed to discern a specified sea roughness. A similar grasp of these factors has been achieved by Walsh [8] using a different theoretical approach in a study of the limitations of airborne beam-limited radars.

III. Signal Processing

Surface roughness information is contained in the slowly and randomly varying envelope and phase functions associated with each carrier. When the illuminated surface has the proper statistical behavior, the instantaneous CW received signals can be represented as

$$e_1(t) = A_1(t) \cos [\omega_1 t + \theta_1(t) + \phi_1]$$

$$e_2(t) = A_2(t) \cos [\omega_2 t + \theta_2(t) + \phi_2]$$

where ω_1 and ω_2 are the respective carrier frequencies, A_1 and A_2 are the Rayleigh distributed envelope fluctuations, and θ_1 and θ_2 are the uniformly distributed phase functions. The constant terms, ϕ_1 and ϕ_2, represent the transmission paths within the instrument and the range to the mean surface.

The general definition of the two frequency correlation function in terms of the signal observables is

$$R(\Delta k) = \frac{\langle A_1 A_2 \exp j(\theta_1 - \theta_2 + \phi_1 - \phi_2)\rangle}{\sqrt{\langle A_1{}^2\rangle\langle A_2{}^2\rangle}}. \quad (7)$$

Previous analysis [1, eq. (24)] has shown this function to be the product of three independent terms. The part of the phase term consisting of $\phi_1 - \phi_2$ is a constant at each Δk and contributes only to the phase of $R(\Delta k)$. Since only the magnitude of R will be measured, these terms will have no effect and can be assumed to be zero for purposes of further discussion. Then, $R(\Delta k)$ can be expressed as

$$R(\Delta k) = \frac{\langle A_1 A_2 \exp j(\theta_1 - \theta_2)\rangle}{\sqrt{\langle A_1{}^2\rangle\langle A_2{}^2\rangle}}$$

$$= \left[\int_{-\infty}^{\infty} p(h) \exp [j2(\Delta k)h]\, dh\right] R_p(\Delta k) \quad (8)$$

with the right hand term arising directly from the electromagnetic field analysis that embodies the specular point summation. The term in brackets is the characteristic function of the specular point height and the Fourier transform of the probability density function. The remaining term is the pattern decorrelation determined in the previous section. The complete statistical description of the surface is contained in the function $p(h)$. In order to avoid the difficulty of measuring the phase term of $R(\Delta k)$ and removing the contribution due to the range, the instrumentation and the pattern term, only the magnitude of $R(\Delta k)$ will be measured. Then, for a known antenna pattern illuminating a stationary statistical surface, $R_p(\Delta k)$ can be computed in a straightforward manner and the magnitude of the characteristic function can be determined from measurements of $|R(\Delta k)|$ as

$$\left|\int_{\infty}^{\infty} p(h) \exp [j2(\Delta k)h]\, dh\right| = \frac{|R(\Delta k)|}{|R_p(\Delta k)|}. \quad (9)$$

This simplification can be justified for conditions of practical interest when there is good reason to believe that $p(h)$ is approximately symmetrical about the mean surface. Should $p(h)$ be slightly unsymmetrical, it could be expressed as the sum of an even and an odd function, $p_e(h)$ and $p_0(h)$. If $p_e(h) \gg p_0(h)$, then the inverse transform of $|R|/|R_p|$ will yield $p_e(h)$ to a close approximation. This leads to the belief that under conditions of near symmetry, since only the relatively small amount of information in $p_0(h)$ is discarded, the rms height and other significant features of $p(h)$ that are of the greatest interest can be discerned from $p_e(h)$ alone.

If just the rms height is of interest, it can be inferred from much less measured data than is needed to obtain the complete probability density function. The derivation presented in Appendix A demonstrates that the rms height is directly proportional to the second derivative of $|R|$ (or $|R|^2$) at $\Delta f = 0$, which can be estimated from relatively few measurements. The rms height is most commonly expressed in terms of the second moment of the p.d.f. of the height variable which, if completely specified, will provide a calculation for $\langle h^2\rangle - \langle h\rangle^2$. Since the square of the magnitude of the transform of $p(h)$ will be the measured quantity, it is desirable to compute these moments from it directly.

Two choices exist in the method of detection that enables the magnitude of the two frequency correlation function to be measured. These are the homodyne detection technique and the simple square law envelope detection method. The homodyne method involves beating each incoming backscattered carrier with a local oscillator that is identical in frequency to the respective transmitted signals. The resulting voltages are

$$v_1(t) = A_1(t) \cos [\theta_1(t) - \alpha]$$

$$v_2(t) = A_2(t) \cos [\theta_2(t) - \beta] \quad (10)$$

where α and β are the net system phase constants, including a phase constant from each local oscillator signal. The presence of this local oscillator phase in each detected signal permits the acquisition of the quadrature components of the incoming RF signal. Expressing $R(\Delta k)$ in terms of the signal functions that contain the information about the surface parameters, (8) becomes

$$R(\Delta k) = \frac{\langle A_1 A_2 \cos(\theta_1 - \theta_2)\rangle + j\langle A_1 A_2 \sin(\theta_1 - \theta_2)\rangle}{\sqrt{\langle A_1{}^2\rangle\langle A_2{}^2\rangle}}. \quad (11)$$

This may be expressed as the sum of real and imaginary components,

$$R(\Delta k) = R_r + jR_i$$

so that the magnitude at each Δk is

$$|R| = \sqrt{R_r{}^2 + R_i{}^2}. \quad (12)$$

An analysis presented in Appendix B demonstrates how $|R|$ can be computed from two correlation measurements between v_1 and v_2, one with arbitrary phase constants α and β and the other with an added 90° shift (plus or minus) introduced on one of them.

A second detection method involves correlating only the fluctuating parts of the squares of the envelopes $A_1(t)$ and $A_2(t)$. This eliminates the need for a coherent L.O. in the receiver. Since the signals have Gaussian statistical properties, it can be shown that this correlation yields $|R|^2$. The detected outputs can be expressed as

$$s_1(t) = A_1^2(t) - \langle A_1^2\rangle$$
$$s_2(t) = A_2^2(t) - \langle A_2^2\rangle. \tag{13}$$

The normalized cross correlation is again computed as

$$C(\Delta f) = \frac{\langle s_1 s_2\rangle}{[\langle s_1^2\rangle\langle s_2^2\rangle]^{1/2}} = |R|^2. \tag{14}$$

The proof of this statement can be found in the comprehensive analysis by Middleton [10]. The accuracy of this relation is not very sensitive to departures of the detector from square law.

This latter method was adopted for the airborne instrument since only one correlation measurement is needed and any phase jitter or noise will not appear in the detected signals to degrade the measurement. Also, the CW signals at f_1 and f_2 can be simulated with long pulses whose bandwidth needs to be much less than the Δf values of interest. Then the different frequency values can be separated by their chosen time sequence without the need to use RF or IF filtering.

IV. Laboratory Experiments

The initial laboratory measurements using a wind-wave tank were performed with a homodyne detection scheme [1]. This system was improved to permit sharper frequency separation at the receiver and more extensive data recording and averaging. The initial measurements were repeated and they demonstrated closer agreement with the theoretical predictions based on measured surface conditions and excellent repeatability and self-consistency. The homodyne method of detection requires that two cross correlations be performed either simultaneously with two quadrature signals or with sequential changes in one local oscillator phase angle to arrive at a quadrature signal. The alternate technique discussed in Section III requires a single correlation between the squared amplitude fluctuations of returning narrow band RF signals, yielding $|R|^2$. Since this method is simpler to implement on a flight experiment, its parallel development in the laboratory was pursued. The redesigned laboratory radar had the capability of readily switching from one method of operation to the other. A block diagram of the amplitude correlation mode of operation is shown in Fig. 2. Measurements with this system were then conducted under identical wind and water surface conditions and the results, presented in Fig. 3, are in good agreement with the theoretical values.

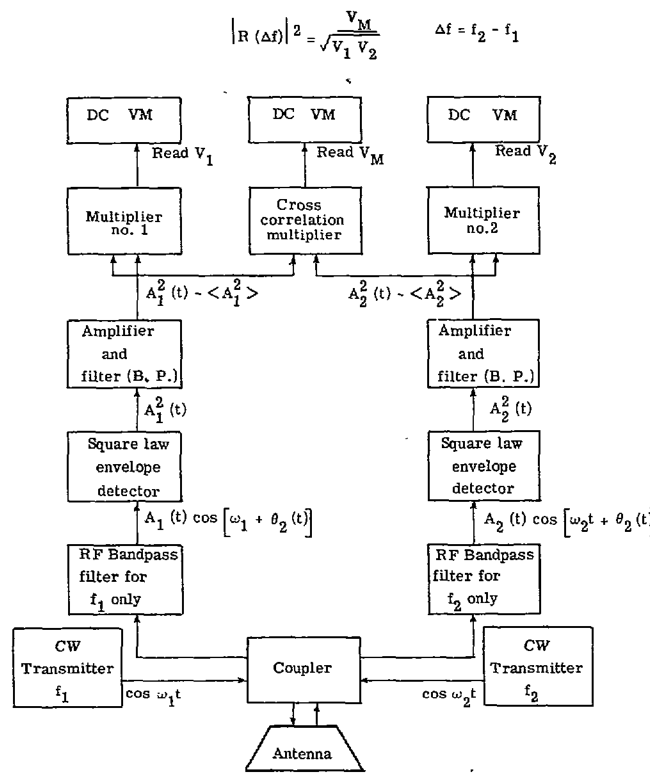

Fig. 2. Block diagram of laboratory radar—amplitude correlation mode.

It was also desirable to observe, to the extent possible in the laboratory, the effects of off nadir alinement and to test the validity of the theory developed in Section II. The antenna alinement was changed from nadir to 7.3° off nadir and measurements of $|R|$ and $|R|^2$ were conducted with both detection techniques. This alinement change constituted about one half of the 3 dB beamwidth and, at this altitude, a strong decorrelation was expected. The measurements agreed closely with the theoretical expectations; the dotted curve in Fig. 3 is an example of these results. More extensive measurements at several different angles of incidence and altitudes were conducted in the flight program and constituted a more thorough study of this effect.

Another important aspect of the laboratory measurement program was the knowledge gained regarding the necessary number of waves and specular points that must lie within the illuminated area at any instant in order to achieve two conditions:

1) provide the reflected signal with Gaussian statistics that is necessary for both the homodyne and amplitude correlation methods of detection to function properly; and
2) provide a population of scatterers that is sufficiently large to give these measurements statistical stationarity and to approximately represent the probability density function of heights of a larger, limiting population that could be obtained from a larger area.

Typical wavelengths in the illuminated region of the wave tank varied from 15 to 25 cm crest-to-crest, and the trans-

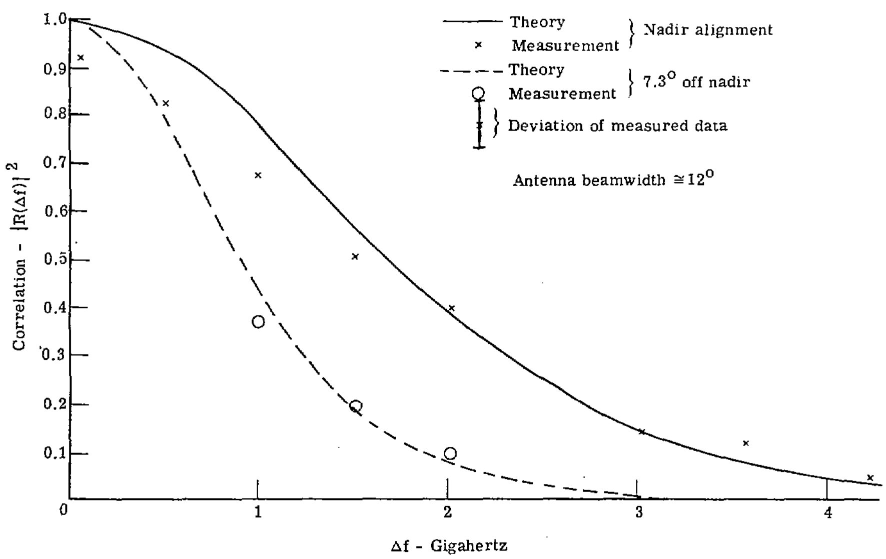

Fig. 3. Measurements and theoretical results for laboratory experiment—amplitude correlation method.

verse crest lengths were about half this distance. The diameter of the illuminated area contained within the half power beamwidth of the antennas is 52 cm. Therefore, at any instant, it seems reasonable to expect that the number of crests inside this illuminated area would be between 4 and 8. Doubling this to account for troughs, yields a total which is not usually considered large when a random population is being studied. However, with respect to the first item mentioned above, studies of random phasor sums by Beckmann [7] have shown that a signal scattered by independently moving statistical objects that have large relative phase differences will have Gaussian statistics to a very close degree when the number of these scatterers exceeds 5. This view is supported by the laboratory observations which showed that the received signal had quadrature components that contained equal power but were uncorrelated. Also the amplitude correlation technique displayed the expected relationship to the homodyne detection and correlation method that is based on having Gaussian signal statistics.

The quantity of interest identified in 2) above is the statistical distribution of the heights of the scatterers. If only a limited population of these points exists in the illuminated area, one wonders how closely the histogram of the heights must conform to the assumed Gaussian (or the p.d.f. that is actually approached in the limit as the area increases indefinitely) to yield valid measurements. The situation may be encountered where the dominant surface wavelength is equal to or greater than the diameter of the illuminated area. This creates a p.d.f. that is a function of time and may deviate appreciably from the ideal limiting p.d.f. Our experimental evidence permits us to draw the following conclusions.

a) The number of wavelengths that lie within the illuminated area at any instant need only be greater than unity to provide a height distribution that is an adequate approximation to the limiting p.d.f. Smaller ratios of wavelength to beam diameter have been observed experimentally, but judgment will be reserved until flight results are completely analyzed.

b) When the condition of a) is met, the observed value of $|R|$ may vary appreciably from the mean. But integrating and averaging these measured values for longer time intervals seems equivalent to increasing the instantaneous population of specular points and provides a better estimate of the limiting value one expects from a strictly stationary and ergodic process.

V. Aircraft Measurements

In order to demonstrate the applicability of the dual-frequency correlation measurement to actual sea surface conditions, an aircraft measurement program using a dual frequency scatterometer (DFS) was begun at the NASA Langley Research Center in the Spring of 1974. Attention was directed to investigating possible limitations due to the nature of the sea surface as well as testing the validity of the theoretical analysis. Data has been collected for low, moderate, and high sea state conditions, and preliminary data reduction has been performed.

The DFS instrument is a modification of an existing scatterometer that operates in a long pulse, beam limited mode and was originally designed to measure average backscattered power. Fig. 4 is a block diagram of that part of the system that is pertinent to the DFS mode of operation. Subsystems required solely for this mode are 1) the controller which provides all of the timing and control signals to the transmitter and receiver, 2) the pulse processor which amplifies the intermediate frequency signal and demodulates the envelope, and 3) the correlator which separates and correlates the amplitude modulations on the returned signals. Pulses are alternately transmitted at $f_a = 13.9$ GHz and $f_b = f_a - \Delta f$, where $0 < \Delta f < 40$ MHz. Calculations by Walsh [8] have shown that the relative positions of the scattering surface and the aircraft may be

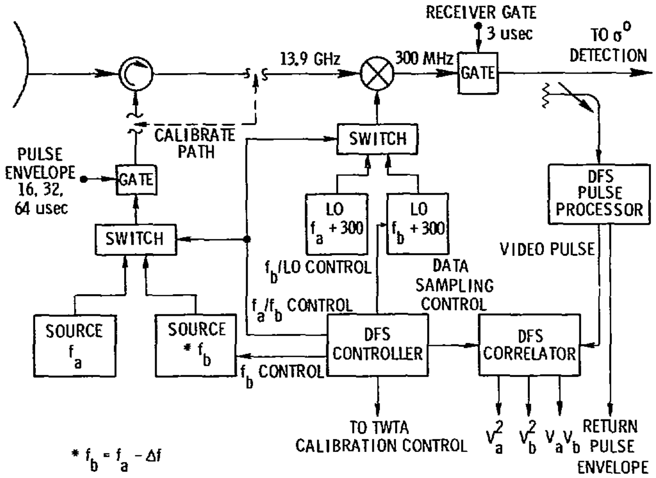

Fig. 4. Dual frequency scatterometer—flight instrument.

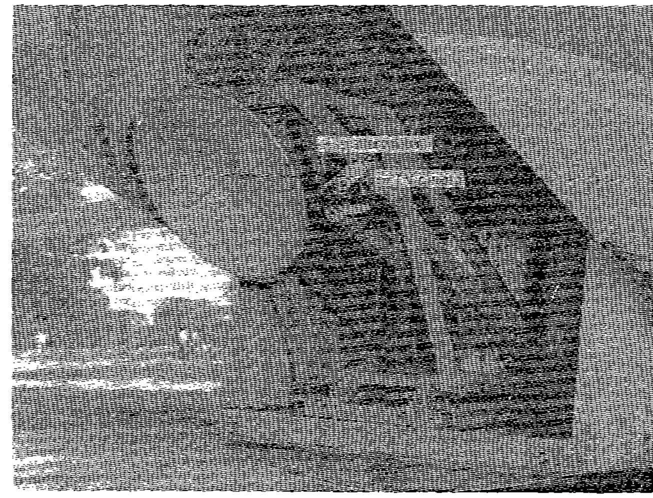

Fig. 5. External view of instrument mounted on aircraft.

assumed to be fixed for intervals less than 1 ms, for the radar wavelength of this system. Therefore a pulse spacing of 80 μs was used to allow consecutive f_a and f_b observations to be considered simultaneous. The various values of Δf are programmable at the DFS controller allowing f_b to be stepped sequentially in as many as 16 increments, where the smallest possible increment is 1 MHz. In the receiver, the f_a and f_b local oscillators are synchronized with the transmitter to maintain a 300 MHz intermediate frequency. The amplitude fluctuations on the f_a and f_b received carriers are detected in the pulse processor, then separated in the correlator and formed into continuous signals using the sample and hold technique. The cross product and self product terms are averaged for 300 ms, and then used to calculate the normalized cross correlation $C(\Delta f)$. This integration time is an important parameter in determining the precision of the correlation value, since it affects the standard deviation (root mean-square error) of a measured estimate. Using statistical data analysis [9], the equation shown below provides an approximation to this standard deviation:

$$\text{S.D.} = \left[\frac{1 + C^2}{2BT}\right]^{1/2}, \qquad 0 \leq C \leq 1$$

where C is the limiting value of the measured correlation, B is the bandwidth of the signal entering the correlator (approximately 300 Hz) and T is the integration time (0.3 s). This value is approximately 0.1 or less, and while not negligible, it does not seriously degrade the observation.

Flight measurements were conducted in June, August, and November of 1974 using the NASA Johnson Space Center NC-130B (NASA 929) aircraft. Fig. 5 is a photograph of the instrument mounted in its measurement position on the lowered cargo ramp of the aircraft. During the course of a complete flight, data were acquired with the aircraft direction successively varied from parallel, 45°, 90°, or 180° with respect to the wave propagation direction. The ground speed was in the 80–95 m/s range for all of the flights, depending on the relative wind speed and direction. Aircraft attitude parameters were recorded so that antenna

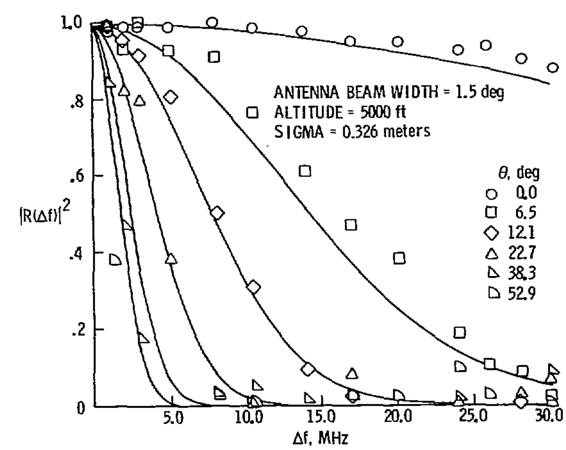

Fig. 6. Flight measurements, June 1974, H = 5000 ft; θ_b = 1.5°; θ_i = off nadir alignment, variable; RMS height inferred from θ_i = 0 data: σ = 0.326 m.

alignment errors could be accounted for. Measurements have been conducted at altitudes of 2000, 5000, and 10 000 ft (610, 3524, and 1049 m) and for incidence angles that varied from nadir to 53°. Two different antenna beamwidths have been used, one of 1.5° and the other of 3.0°. Laser wave profile data were obtained from an altitude of 100 m on each flight for comparison with the DFS results. During the June flights in the central Atlantic off the east coast of the U.S., smooth sea conditions ($H_{1/3} \cong 1.0$ m) existed. In August, a tropical depression, which later became hurricane Carmen, formed in the Caribbean and provided the opportunity to conduct measurements with $H_{1/3} \cong 2.8$ m. The highest sea state conditions thus far ($H_{1/3} \cong 6.1$ m) were seen in the North Sea during November. Typical results from the June 1974 flights are shown in Figs. 6, 7, and 8. Measurements at nadir ($\theta_i = 0$) barely detect the presence of the very small roughness. Fitting the theoretical curves to the data indicates an rms wave height of about 0.3 m. Significantly, the data sets for off nadir angles follow the theoretical predictions with regard to decorrelation versus frequency separation. Comparing Figs. 6 and 7, a stronger decorrelation effect is seen at 10 000 ft than at

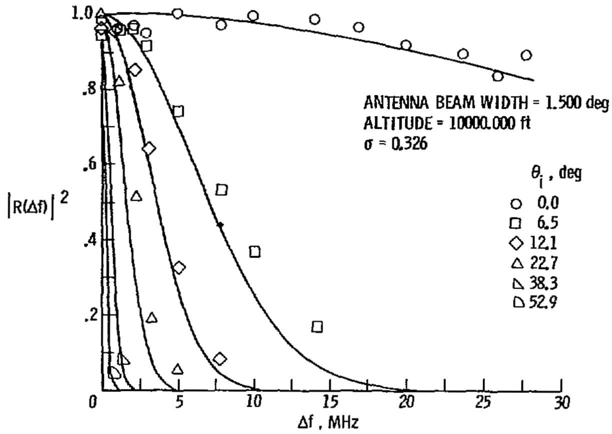

Fig. 7. Flight measurements, June 1974, $H = 10\,000$ ft; $\theta_b = 1.5°$; θ_i = off nadir alignment, variable; RMS height inferred from $\theta_i = 0$ data: $\sigma = 0.326$ m.

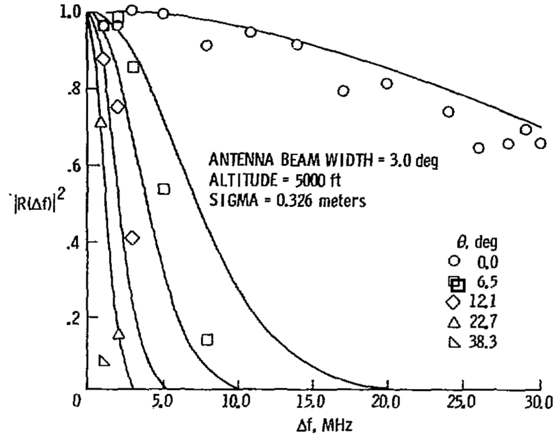

Fig. 8. Flight measurements, June 1974, $H = 5000$ ft; $\theta_b = 3.0°$, θ_i variable, theoretical curves use $\sigma = 0.326$ m.

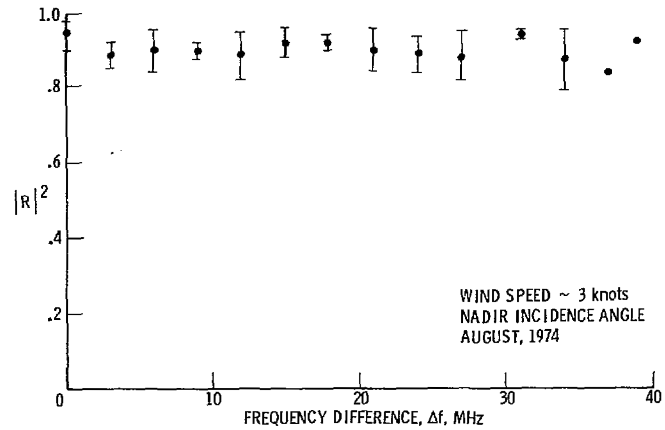

Fig. 9. Flight measurements, August 1974, low sea state, $H = 5000$ ft, $\theta_b = 1.5°$.

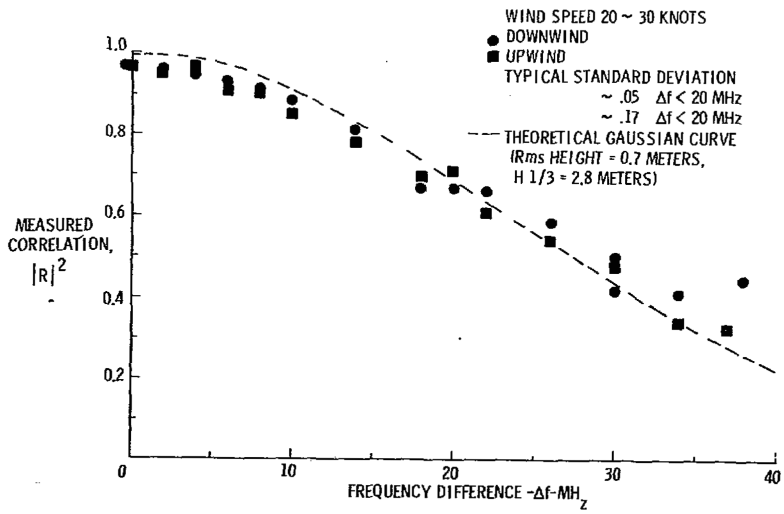

Fig. 10. Flight measurements, August 1974, moderate sea state, $H = 10\,000$ ft, $\theta_b = 1.5°$.

5000 ft due to the induced range spreading of the scatterometer. Figs. 6 and 8 show the same phenomena induced by enlarging the antenna beamwidth from 1.5° to 3.0° at a fixed altitude. During one mission in early August, extremely smooth seas were encountered from 5000 ft using the narrow beamwidth, and these conditions resulted in a negligible decorrelation, compared with the natural data scatter (Fig. 9).

The moderately rough sea results were acquired near a storm in the Caribbean in late August. The data shown in Fig. 10 are in excellent agreement with a theoretical curve using an rms height estimated from laser wave profile data.

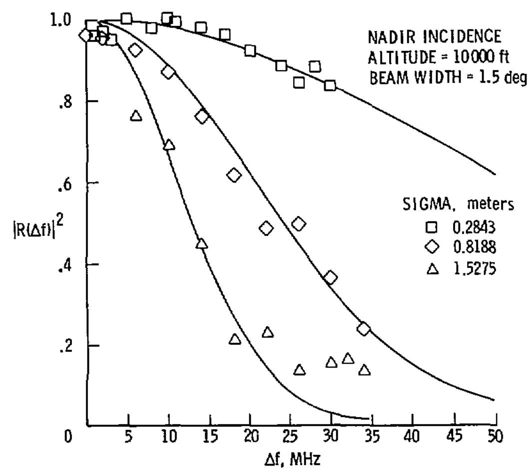

Fig. 11. Flight measurements, comparison of North Sea results (November, 1974) with lower sea state observations, $H = 10\,000$ ft, $\theta_b = 1.5°$.

An upwind and a downwind run are presented, and as expected flight direction has no affect on this measurement. Two flights over the North Sea in late autumn provided an additional moderate sea state case and one high sea state condition. These results are contrasted with each other and one of the low sea state measurements in Fig. 11. The solid theoretical curves shown here take into account all beam and platform geometry and are computed using an rms wave height that provides the best fit to the data of each set. Each data point is the mean of ten independent correlation measurements at that Δf. Surprisingly, the data set for high sea state shows that the correlation at the larger Δf does not fall off as rapidly as expected based on a Gaussian distribution of specular point elevations. This effect may well be due to the limited diameter of the illuminated area (about 250 ft at an altitude of 10 000 ft) which is smaller than the larger surface wavelengths that dominate the surface roughness. This condition could result in a large variation in the specular point height extent during a particular observation period. Walsh [6] has been studying this restriction on beam limiting radars. Future flights are planned to evaluate this contention and explore this effect further.

VI. Concluding Remarks

Progress has been made in understanding the underlying theory of this technique and applying this measurement to the ocean surface using an airborne instrument. Results to date have demonstrated the accuracy and simplicity of the measurement and data reduction procedures. Using the carrier envelope correlation method, no correction or concern for aircraft altitude fluctuations is needed. Optimum instrument design information is now available.

Some uncertainties due to the character of the ocean surface still need to be explored further, such as the possible effect of large foam coverage or spray and the relation between the ocean wavelength and the illuminated area diameter. Effort is continuing to obtain highly accurate wave height statistics from laser profilometer measurements for comparison with these results. The influence of precipitation between the aircraft and the surface should also be evaluated experimentally. A sensor operating at this microwave wavelength should have advantages over optical or laser techniques in heavy precipitation or other unfavorable conditions which make low flying surveys difficult or undesirable. It is expected that future missions will yield definitive answers to these qûestions and further support the conclusions drawn from the results presently available.

Appendix A

Direct Determination of RMS Height Alone

Since

$$R(\Delta k) = \int_{-\infty}^{\infty} p(h)[\exp j2(\Delta k)h]\, dh \tag{A1}$$

then

$$\begin{aligned}|R(\Delta k)|^2 &= R(\Delta k)R^*(\Delta k)\\ &= \int_{-\infty}^{\infty}\int_{-\infty}^{\infty} p(u)[\exp j2(\Delta k)u]\, p(v)\\ &\quad\cdot [\exp -j2(\Delta k)v]\, du\, dv.\end{aligned} \tag{A2}$$

If this double integral is differentiated twice with respect to $(2\Delta k)$, and evaluated at $\Delta k = 0$, it follows that

$$-\frac{1}{2}\frac{d^2(|R|^2)}{d(2(\Delta k))^2} = \langle h^2\rangle - \langle h\rangle^2. \tag{A3}$$

Measurements of $|R|^2$ versus Δf can readily yield the second derivative at the origin which is then scaled to provide the right hand side of this equation. This result demonstrates that the correlation measurements can be used directly to determine the rms wave height, independently of the symmetry of $p(h)$ and without having to perform an inversion to obtain the functional form of $p(h)$.

Appendix B

Determination of $|R|$ from Homodyne Detected Signals

Consider the normalized cross correlation,

$$C(\Delta f) \triangleq \frac{\langle v_1 v_2\rangle}{[\langle v_1{}^2\rangle\langle v_2{}^2\rangle]^{1/2}} \tag{B1}$$

where v_1 and v_2 are given in (10). Keeping in mind that A_1 and A_2 are Rayleigh distributed while θ_1 and θ_2 are uniformly distributed over a 2π rad range, it then follows that

$$\langle v_1{}^2\rangle = \frac{\langle A_1{}^2\rangle}{2} \quad\text{and}\quad \langle v_2{}^2\rangle = \frac{\langle A_2{}^2\rangle}{2}. \tag{B2}$$

The numerator term can be expanded as

$$\langle v_1 v_2\rangle = \langle A_1 A_2 \cos(\theta_1 - \alpha)\cos(\theta_2 - \beta)\rangle \tag{B3}$$

$$\begin{aligned}&= \tfrac{1}{2}\langle A_1 A_2 \cos[(\theta_1 - \theta_2) - (\alpha - \beta)]\rangle\\ &\quad + \tfrac{1}{2}\langle A_1 A_2 \cos(\theta_1 + \theta_2) - (\alpha + \beta)\rangle.\end{aligned} \tag{B4}$$

The second term vanishes because averaging for the amplitudes can be separated from the term containing $\theta_1 + \theta_2$, and the latter averages to zero for any amount of correlation between these phases. The remaining term can be expanded as

$$\langle v_1 v_2 \rangle = \tfrac{1}{2}\langle A_1 A_2 \cos(\theta_1 - \theta_2)\rangle \cos(\alpha - \beta) + \tfrac{1}{2}\langle A_1 A_2 \sin(\theta_1 - \theta_2)\rangle \sin(\alpha - \beta). \quad \text{(B5)}$$

Therefore the normalized correlation becomes

$$C(\Delta f) = R_r(\Delta f)\cos(\alpha - \beta) + R_i(\Delta f)\sin(\alpha - \beta). \quad \text{(B6)}$$

Since the value of $(\alpha - \beta)$ is unknown as is the ratio of R_i and R_r, a measurement of $C(\Delta f)$ is not sufficient to infer $|R|$. However, if just one phase term α or β is shifted by plus or minus 90°, and the new correlation value $C'(\Delta f)$ is measured, this information combined with $C(\Delta f)$ can yield $|R(\Delta f)|$, since

$$[C(\Delta f)]^2 + [C'(\Delta f)]^2 = R_r^2 + R_i^2 = |R(\Delta f)|^2. \quad \text{(B7)}$$

This analysis demonstrates how $|R|$ can be determined by measuring two cross correlations between homodyne detected signals under simple phase quadrature conditions on one of the local oscillators.

Acknowledgment

The authors wish to express their appreciation for the important contributions of their colleagues at NASA Langley: Mr. J. C. Fedors and the late Dr. J. Q. Howell who developed the DFS flight instrument, Mrs. S. O. Edge who developed computer programs for the processing of the flight data, and Dr. W. L. Jones, Dr. C. T. Swift, and Mr. W. L. Grantham whose efforts contributed to the success of the flight programs.

References

[1] D. E. Weissman, "Two frequency radar interfecometry applied to the measurement of ocean wave height," *IEEE Trans. Antennas Propagat.*, vol. AP-4, pp. 649–656, Sept. 1973.
[2] J. E. Seltzer, "Spatial densities for specular points on a Gaussian surface," *IEEE Trans. Antennas Propagat.*, vol. AP-20, pp. 723–731, Nov. 1972.
[3] D. Barrick, "Determination of rms height of a rough surface using radar waves," Antenna Lab., Ohio State University, Columbus, Rep. 1388-19, Aug. 1965.
[4] R. Kodis, "A note on the theory of scattering from an irregular surface," *IEEE Trans. Antennas Propagat.*, vol. AP-14, pp. 77–82, Jan. 1966.
[5] B. S. Yaplee *et al.*, "Nanosecond radar observations of the ocean surface from a stable platform," *IEEE Trans. Geosci. Electron.*, vol. GE-9, pp. 170–174, July 1971.
[6] E. J. Walsh, "Limitations on oceanographic use of beam-limits target referenced radars," to be published in *IEEE Trans. Antennas Propagat.*
[7] P. Beckman, *Probability in Communication Engineering.* New York: Harcourt, 1967, ch. 4.
[8] E. J. Walsh, private communication.
[9] J. S. Bendat and A. G. Piersol, *Random Data: Analysis and Measurement Procedures.* New York: Interscience, 1971, sect. 6.4.
[10] D. Middleton, *Introduction to Statistical Communication Theory.* New York: McGraw-Hill, 1960, sect. 9.1-1.